Chapter 1

Introduction

1.1 Dwarf galaxies: an introduction

Dwarf galaxies, with masses around $10^9\ M_\odot$, represent the smallest galaxies known in the universe. Despite their small size, the term 'dwarf galaxy' is not defined by their dimensions but rather by their luminosity. These galaxies appear faint compared to larger counterparts like the Milky Way. They often exhibit irregular shapes and occasional elongation due to interactions. Therefore, the defining criterion for identifying dwarf galaxies lies in their luminosity rather than their size. Their luminosity has an upper limit with an absolute visual magnitude, $M_V \approx -18$, while at the lower end, they are notably more luminous than typical globular clusters in the Milky Way, implying $M_V < -8$ [1]. Similar to the prevalence of less massive stars compared to the luminous massive ones, these small galaxies are also numerous [2–4]. They are chemically less evolved compared to larger galaxies and therefore retain a significant portion of their original elemental composition. Consequently, they serve as fundamental building blocks for larger galaxies through merging processes [5].

Dwarf galaxies manifest diverse morphological classifications. Based on their gas content and ongoing star formation rates, they are broadly categorized into three types: dwarf Spheroidal (dSph), dwarf Irregular (dIrr), and blue compact dwarf (BCD) galaxies. Within our Local Group, there is a significant presence of dwarf spheroidal galaxies. These entities, extremely faint in nature, pose challenges in detection. Typically, dwarf spheroidals exhibit negligible gas content and have remained devoid of star formation for several hundred million years or longer [6]. In contrast, dwarf irregulars, the objects of interest of this thesis, hold a substantial gas content, accompanied by some ongoing star formation activities, distinguishing them from dwarf spheroidals. These galaxies commonly display exponential

surface brightness profiles. BCDs, also characterized by abundant gas reserves, demonstrate intense ongoing star formation processes.

1.2 The Interstellar Medium

1.2.1 A brief overview of the interstellar medium in galaxies

The medium between stars, known as the Interstellar Medium (ISM), is a crucial component of galaxies as it is the ISM which is responsible for the formation of stars through the process of gravitational collapse. Despite dark matter currently accounting for the majority of a galaxy's mass, the baryonic matter, constituting around 10% of the total mass, governs the observable characteristics of galaxies. In the early stages of galactic evolution, all this baryonic mass predominantly existed in the form of gas within the ISM. Over time, as galaxies evolve, the ISM undergoes transformation, with a portion converting into stars, and some being expelled as galactic winds. In the present epoch of our galaxy, the Milky Way, approximately 10% of baryons remain in the ISM, while the rest has been incorporated into stars or their remnants [7]. The ISM itself manifests in two primary forms:

- Interstellar Gas: This constitutes the predominant fraction of the ISM, making up about 90% of its total mass. Interstellar gas primarily comprises hydrogen and helium.
- Interstellar Dust: Composed of minute particles containing heavier elements like silicon (Si) and carbon (C), interstellar dust represents a smaller fraction, approximately 10% of the ISM's composition. It is intricately mixed with the interstellar gas.

In addition to the primary components of interstellar gas and interstellar dust, the ISM contains various other components, briefly outlined below ([7], and references therein):

- Cosmic rays: These are ions and electrons characterized by relativistic kinetic energies.
- Interstellar radiation field: This field is composed of photons originating from various sources, including the cosmic microwave background (CMB), light emitted by stars, thermal emission from interstellar dust grains heated by starlight, synchrotron radiation from relativistic electrons, free-free emission (bremsstrahlung) from interstellar plasma etc.
- Interstellar magnetic field: Originating from electric currents in the ISM, the interstellar magnetic field guides the trajectories of cosmic rays, influencing their behavior.

- Gravitational field: Arising from all forms of matter in the galaxy, including ISM, stars, stellar remnants, and dark matter, the gravitational field is a fundamental force shaping the structure and dynamics of the galactic system.

The ISM exhibits a dynamic nature and is observed in distinct phases characterized by varying temperatures and densities. These phases are briefly described below ([7], and references therein):

- Hot Ionized Medium (HIM): The HIM represents a phase within the ISM characterized by extremely high temperatures, equal to or exceeding $10^{5.5}$ K. This intense heat is primarily a result of shock waves generated by supernova explosions. The gas in the HIM is collisionally ionized, exhibiting a notably low number density, approximately 0.004 cm^{-3}. Despite its low density, the HIM occupies a substantial portion, nearly half, of the total volume of the ISM. Detection of the HIM is achieved through observations in the Ultraviolet (UV) and X-ray emissions. These regions typically have characteristic dimensions of around $\sim$ 20 pc and undergo cooling processes over $\sim$ Myr timescales. Due to its similarity of temperature and ionization state with the solar corona, HIM is often referred to as "coronal gas".

- H II gas: It constitutes a significant phase within the vast and complex environment of the ISM. In this phase, hydrogen atoms undergo a process of photoionization, driven by the powerful UV radiation emitted by hot and young O-type stars. This ionized state of the gas manifests in two primary forms, each with distinct characteristics. Firstly, we have the H II regions, which are dense clouds with a number density of $\sim 10^4$ cm^{-3}. An example is the prominent Orion Nebula in our galaxy. These regions are relatively compact, with typical dimensions spanning a few pc. H II regions have a finite lifespan, generally ranging from approximately 3 - 10 Myr. Their existence is intricately linked to the presence of massive, short-lived O-type stars, whose intense radiation is responsible for both ionizing the hydrogen within these regions and shaping their dynamic evolution. Secondly, the Warm Ionized Medium (WIM) represents a diffuse phase with lower density ($\sim$ 0.3 cm^{-3}) compared to the H II regions. Within the ISM, about 90% of ionized hydrogen is found within the WIM phase. Unlike the confined nature of H II regions, the WIM pervades the interstellar space in a more dispersed manner. The temperature of this ionized phase is around 10^4 K. Apart from these H II regions and the WIM, ionized gas also contributes to the formation of structures known as Planetary Nebulae. These nebulae emerge as a consequence of stellar evolution, particularly during the final stages of stars with initial masses ranging from $0.8M_\odot$ to $6M_\odot$. The process involves the shedding of mass, exposing the hot

stellar core. The intense radiation originating from this exposed core photoionizes the surrounding outflowing gas, creating the visually beautiful planetary nebulae. Over time, these nebulae gradually fade away, their observable lifespan extending to $\sim 10^4$ Myr. These regions can be observed through optical line emission and thermal radio continuum.

- Warm Neutral Medium (WNM): The WNM predominantly comprises of atomic hydrogen (HI) that has been heated to a temperature of approximately 10^4 K. It exhibits a number density of around 0.6 cm^{-3}. The WNM occupies nearly 40% of the ISM and is primarily observable through the 21 cm emission line.

- Cold Neutral Medium (CNM): This is another significant component of the ISM consisting mainly of atomic hydrogen but at lower temperatures compared to the WNM, with a temperature of approximately 100 K. It exhibits a number density of around 30 cm^{-3} and occupies roughly 1% of the volume of the ISM. This particular phase can also be primarily observed using the 21 cm emission line.

- Dense Molecular Clouds: It represents the coldest and most densely populated component of the ISM, characterized by temperatures ranging from 10 to 50 K and number densities around $10^3 - 10^6$ cm^{-3}. This phase predominantly consists of molecular hydrogen (H_2) and serves as the primary region for star formation. These clouds are gravitationally bound and can be observed in CO band and Far Infrared (FIR) emissions associated dust grains.

1.2.2 Interstellar dust

As a substantial portion of the work in this thesis revolves around the interstellar dust component of the ISM, so the following few sections extensively explores the different properties associated with interstellar dust.

The discovery of interstellar dust within the ISM can be attributed to the pioneering work of R. J. Trumpler in 1930, during his investigation of the properties of star clusters [8]. As previously mentioned, these dust grains consist of tiny solid particles composed of heavy elements such as silicon (Si), carbon (C), oxygen (O), iron (Fe) etc. These heavy elements are periodically injected into the ISM through the explosions of massive stars. Within the ISM, dust grains are thoroughly mixed with the interstellar gas and can be found in all phases except the hot ionized medium. Their sizes range from a few molecules to a few microns.

Despite their relatively negligible contribution to the overall mass of the ISM ($\sim 10\%$), dust grains play a pivotal role in shaping our understanding of the universe by obscuring starlight which is believed to emerge from the combination of scattering and absorption, collectively referred to as Extinction. They scatter a significant portion of incident radiation, leading to diffuse emissions primarily observed in the Far Ultraviolet (FUV) regime. The remaining fraction of radiation at shorter wavelengths (optical and UV) is absorbed and subsequently re-emitted at longer wavelengths, resulting in diffuse emissions in the Infrared (IR) and sub-millimeter wavelengths. It has been estimated that 30% or more of the energy emitted by stars in the universe is re-radiated by dust in the infrared [9].

Thus, dust grains exert control over the thermodynamics of galaxies and influence the dynamics of star formation. Additionally, dust serves as sites for the formation of H_2 molecule within the ISM. Therefore, the study of dust grains and their properties has become a vital field of research in order to comprehend the processing of starlight and star formation processes within galaxies.

1.2.3 Extinction by dust grains

The initial evidence in favour of the presence of interstellar dust came from Extinction, which refers to the obscuration of starlight [8]. Extinction causes attenuation in the observed flux (or an increase in magnitude) of light emitted by astrophysical objects resulting from the combination of two processes: scattering and absorption. This attenuation is wavelength-dependent and is more pronounced at shorter wavelengths (blue) compared to longer wavelengths (red). This phenomenon is commonly known as “reddening”. Therefore, it is of utmost importance to correct for the effects of extinction by interstellar dust grains in order to have a proper understanding of the intrinsic properties of any astrophysical object.

The measurement of extinction in stars can be achieved through the “pair method”, which involves comparing the spectrophotometry of two stars belonging to the same spectral class. By selecting one star that does not experience any extinction and another star that is significantly reddened, we can quantify the extinction effect. If we denote the magnitude of the unextincted star as m_1 and the magnitude of the reddened star as m_2, then

$$m_{1\lambda} = -2.5log(f_{1\lambda}) + C \tag{1.1}$$

$$m_{2\lambda} = -2.5log(f_{2\lambda}) + C + A_\lambda \tag{1.2}$$

where, $f_{1\lambda}$ and $f_{2\lambda}$ represent the fluxes of the stars at a specific wavelength λ, and C is a constant for stars of the same spectral class. The term A_λ in Equation 1.2 is the extinction in magnitudes suffered by the star at the given wavelength λ. By utilizing the above equations, we can derive A_λ as:

$$A_\lambda = 2.5log(\frac{f_{2\lambda}}{f_{1\lambda}}) + \Delta m_\lambda \tag{1.3}$$

Here, Δm_λ represents the magnitude difference between the stars. The difference in extinction at two different wavelengths is given by

$$A_B - A_V = (B-V) - (B-V)_0 \tag{1.4}$$

In the equation, the term $(B-V)$ represents the observed difference between the B and V magnitudes, while $(B-V)_0$ represents their intrinsic difference. In the Johnson UBV system, B corresponds to a wavelength of 4400 Å, and V corresponds to 5500 Å. The difference in extinction between these magnitudes is commonly known as the color excess (E(B-V)). The pair method has proven to be effective in measuring extinction at different wavelengths along various lines of sight, allowing to derive "extinction curves" spanning a range of wavelengths from near-IR (NIR) to UV. These extinction curves provide valuable insights into the properties of dust grains in the ISM of galaxies [10]. The ratio of the total to selective extinction, denoted by $R_V = A_V/(A_B - A_V)$, serves as a measure of the slope of the extinction curve in the optical region. When $R_V \to \infty$, it suggests the presence of very large grains, while $R_V \approx 1.2$ indicates Rayleigh scattering ($A_\lambda \propto \lambda^{-4}$) by dust grains that are much smaller than the wavelength. Higher values of R_V may indicate the possibility of grain growth through accretion [11]. In the Milky Way, the value of R_V varies significantly along different lines of sight, ranging from 2.1 (as observed towards HD 210121) [12] to as high as 5.6 - 5.8 (as measured in the direction of HD 36982) [13, 14]. However, the average extinction in the diffuse regions of the Milky Way is characterized by an R_V value of approximately 3.1 [13, 15].

Scattering

Scattering refers to the change in the direction of incident radiation, and this change is influenced by the composition, shape, and size of the dust grains acting as the scatterers. The quantity of radiation scattered by these particles is described by a parameter known as albedo (α), which can be defined as follows:

$$\alpha = \frac{Q_{sca}}{Q_{ext}} \tag{1.5}$$

where, Q_{sca} is the scattering efficiency factor and Q_{ext} is the total extinction efficiency factor. Albedo ranges from 0 to 1 where 0 indicates no scattering and 1 indicates complete scattering. If the relative distribution of the stars and the dust grains are known, we can calculate the amount of scattered radiation in the following way:

The amount of energy incident on a volume element of dust dV is given by

$$E_{inc} = \frac{L}{4\pi d^2} \times \sigma_{ext} \times ndV \tag{1.6}$$

where L is the luminosity of the star, d is the distance between the star and the dust grain, σ_{ext} is the extinction cross section which depends on the shape, size and composition of the grains and n is the number density of the dust grains. Then the amount of scattered radiation in all directions is given by

$$E_{sca} = \alpha \times E_{inc} \tag{1.7}$$

The amount of scattered radiation into unit solid angle about a direction θ is written as

$$E_{sca}(\theta) = \alpha \times E_{inc} \times \phi(\theta) \tag{1.8}$$

where $\phi(\theta)$ is called the scattering phase function which represents the amount of energy scattered into a solid angle about a direction θ.

The scattering phase function $\phi(\theta)$ is given by

$$\phi(\theta) = \frac{1}{\sigma_{sca}} \times \frac{d\sigma}{d\Omega} \tag{1.9}$$

In this equation, σ_{sca} is the total scattering cross section integrated over all directions and $\frac{d\sigma}{d\Omega}$ represents the differential scattering cross section.

The direction of scattering is described by another parameter called the phase function asymmetry factor (g) which is given as follows:

$$g = \frac{\int cos\theta\phi(\theta)d\omega}{\int \phi(\theta)d\omega} \tag{1.10}$$

The phase function asymmetry factor (g) varies within the range of -1 to +1, including of 0. A value of g = 0 represents isotropic scattering, meaning the incident radiation is scattered uniformly in all directions. A value of g = -1 corresponds to complete back scattering, implying a 180° deflection of the incident radiation. On the other hand g = +1

indicates strong forward scattering, where the incident radiation undergoes no deflection at all.

When electromagnetic radiation encounters a dust grain made up of discrete electric charges, the electric field of the radiation induces oscillatory motion in these electric charges within the dust grain. These oscillating charges emit electromagnetic energy in all directions, sharing the same frequency as the incident radiation. Consequently, the frequency of the incident radiation remains unchanged during scattering. When the size of the scattering particle 'a' (assuming a spherical shape for simplicity), is significantly smaller than the wavelength λ of the incident radiation, this type of scattering is termed Rayleigh scattering. Conversely, when the particle sizes are comparable to the wavelength, Mie theory becomes applicable. In the context of scattering by interstellar dust at optical and UV wavelengths, Mie theory proves more relevant due to the sizes of dust grains being comparable to the wavelength of the incident radiation. The extinction efficiency factor, Q_{ext}, depends on two dimensionless parameters: $Q_{ext} = Q_{ext}(x,m)$, where $x = 2\pi a/\lambda$, and m represents the refractive index of the material constituting the dust grain. The condition $x \ll 1$ corresponds to Rayleigh scattering, while Mie scattering occurs otherwise. Q_{ext} can be expressed as a series expansion in the powers of x, forming a convergent series. For extremely large particles ($x \to \infty$), the extinction cross-section equals precisely twice the geometrical cross-section (Q_{ext} = 2). This result arises from the diffraction of light at the edges of the particle, leading to additional small-angle scattering.

Absorption

The unscattered radiation is absorbed by the dust grains, resulting into an increase in the internal energy of the grains. This absorption process is complementary to the scattering process. The absorbed radiation is subsequently re-emitted at longer wavelengths, depending on the temperature of the dust grains. The temperature of the dust grains (T_d) can be determined from the equilibrium of the absorbed and emitted radiation. If we consider a star with a luminosity of L and a distance d between the star and the dust grains, the energy incident on a volume element of dust (dV) with a number density of n can be expressed as

$$E_{inc} = \frac{L}{4\pi d^2} \times \sigma_{ext} \times ndV \tag{1.11}$$

The amount of radiation absorbed by the volume element dV is

$$E_{abs} = (1-\alpha) \times E_{inc} \tag{1.12}$$

Here, α is the albedo of dust grains which characterizes the amount of scattered radiation.

This absorbed energy is subsequently radiated at longer wavelengths and can be mathematically represented as

$$E_{rad} = 4\pi \times ndV \times \sigma_B {T_d}^4 \tag{1.13}$$

where T_d represents the equilibrium dust temperature and σ_B is the Stefan-Boltzmann constant. With the assumption that the dust grains emit radiation like a perfect black body and follows Kirchhoff's law, the emissivity is equal to the absorptivity. Therefore,

$$E_{abs} = E_{rad} \tag{1.14}$$

which gives the equilibrium dust temperature as

$$T_d = \left[\frac{L(1-\alpha)}{16\pi d^2 \sigma_B}\right]^{1/4} \tag{1.15}$$

If we have more than one stars with luminosities $L_1, L_2, L_3...$ at distances $d_1, d_2, d_3...$ from the dust grains, then the equilibrium temperature is given by

$$T_d = \left[\frac{\left[\frac{L_1}{{d_1}^2} + \frac{L_2}{{d_2}^2} + \frac{L_3}{{d_3}^2} + ...\right] \times (1-\alpha)}{16\pi\sigma_B}\right]^{1/4} \tag{1.16}$$

Then, the energy radiated at a wavelength λ is written as:

$$E_{rad}(\lambda) = 4\pi \times ndV \times B_\lambda(T_d) \times \sigma_{abs} \tag{1.17}$$

where σ_{abs} is the absorption cross section of the dust grains and $B_\lambda(T_d)$ is the Planck's function given by

$$B_\lambda(T_d) = \frac{2hc^2}{\lambda^5} \frac{1}{exp(\frac{hc}{\lambda k_B T_d}) - 1} \tag{1.18}$$

Here, h is the Planck's constant, k_B is the Boltzman's constant and c is the speed of light in vacuum.

1.2.4 Formation and evolution of dust grains

Dust grains are formed as a result of the condensation of rapidly cooling gas in stellar outflows [16, 17]. These grains are commonly referred to as "stardust". Various astrophysical

sources, including Asymptotic Giant Branch (AGB) stars, supernovae (SNe), novae, red supergiants, and Wolf Rayet stars, play significant roles in the production of these dust grains [18]. It is believed that the stardust present in the Milky Way and the Magellanic Clouds primarily originates from AGB stars [10, 18, 19]. However, in the early Universe, SNe played a more prominent role in stardust production compared to AGB stars, as the typical timescale for stars to reach the AGB phase ($\sim$ 1 Gyr) exceeds the cosmic timescale during the early Universe ([20] and references therein). Interestingly, the initial detection of stardust formed by SNe, observed in sub-millimeter wavelengths with *SCUBA* in the remnants of Cassiopeia A and Kepler supernovae, revealed a much larger mass (a few $M_{\odot}$) than expected theoretically [21, 22]. However, recent observations in the IR by the *Spitzer Space Telescope* and *AKARI*, along with sub-millimeter observations, have shown better agreement with the theoretical expectation of stardust mass ($0.01 - 0.1 M_{\odot}$ per supernova) [23–25].

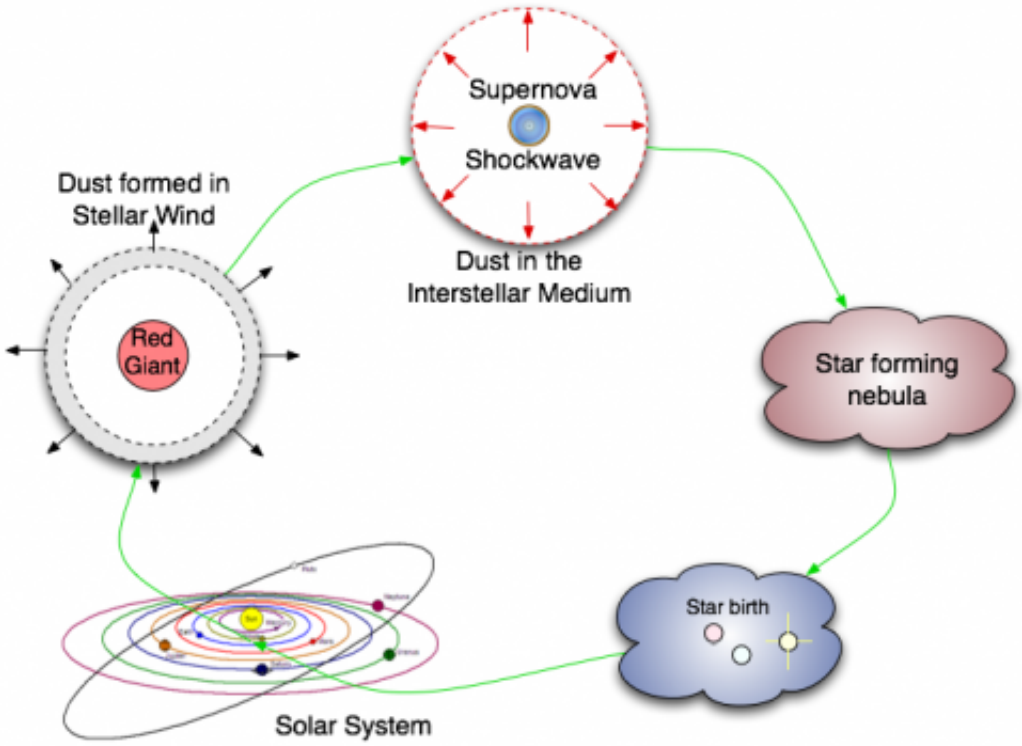

Fig. 1.1 An schematic diagram of the life cycle of interstellar dust grains (Image credit: *Herschel Space Observatory*)

After being injected into the ISM from the stellar outflows, dust grains undergo various interstellar processes that lead to their evolution and eventual destruction. Grains present in hot gas suffer sputtering as a result of bombardment by thermal protons, leading to erosion

of the grains [16, 26]. Additionally, dust grains may get destroyed by grain-grain collisional shattering caused by SNe shock waves [20]. Although dust grains initially form in stellar outflows, the majority of dust grains found in the ISM were not produced through this mechanism. Instead, their composition is determined by the processes they undergo within the ISM. Hence, most of the interstellar dust is not classified as stardust. Considering the destruction efficiency, the estimated theoretical lifespan of dust grains is approximately 100 Myr [27–29], whereas the insertion time of stardust into the ISM is around 1 billion years [18]. Therefore, maintaining the abundance of dust in galaxies requires an additional efficient mechanism for dust production beyond those mentioned previously. The most plausible mechanism is grain growth within dense molecular clouds through the accretion of atoms and molecules onto the surface of existing grains, leading to a transition from the gaseous to the solid phase [10, 27]. This process of accretion growth increases the mass of dust in the ISM and can also account for the depletion of elements in the gaseous phase of the ISM [20]. Thus, the destruction of dust grains is balanced by the growth of grains through the accretion process, ensuring the maintenance of dust abundance in galaxies. Fig. 1.1 provides a schematic diagram illustrating the life cycle of interstellar dust grains.

The evolutionary picture of dust grains begins with a small silicate core formed in the atmospheres of cool stars. Once ejected into the ISM and cooled to 10-15 K, these cores facilitate the growth of mantles composed of solid H_2O or ice. As these silicate cores are captured in dense molecular clouds, they gradually build up an inner mantle of organic refractory materials. These materials are produced by the photoprocessing of volatile ices by UV photons from hot stars and stellar winds. Within the dense molecular clouds, once a critical density is reached, star formation occurs, leading to the ejection of some cloud material into the surrounding space. This material expands into diffuse clouds when it finds itself in a low-density environment. During this transition from high to low-density phases, the volatile grain mantles undergo extensive photoprocessing, producing most of the organic refractory material. It is important to note that without these organic refractory materials, the silicate cores would not survive. The organic refractory mantle in a dust grain is not homogeneous but rather layered, similar to the rings of a tree trunk. Sequential mantle formation in molecular clouds and intense photoprocessing in diffuse clouds create a structure in which the innermost layer is heavily irradiated, surrounded by more lightly photoprocessed ices with first-generation refractory materials. In diffuse clouds, a dust grain can be pictured as a multilayered particle with a silicate core of average radius $0.05\ \mu$m, surrounded by a mantle of average thickness $0.05\ \mu$m (total thickness $0.1\ \mu$m). However, in

dense molecular clouds, there is an additional mantle of ices along with other materials. This structure of dust grains is known as the core-mantle structure ([30] and references therein).

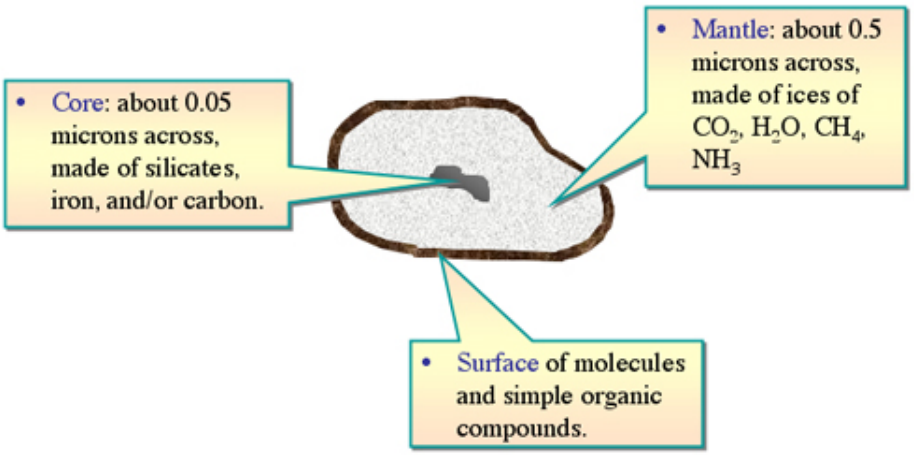

Fig. 1.2 The Core-Mantle structure of interstellar dust grains (Image credit: https://astronomy.swin.edu.au/cosmos/D/Dust+Grain)

1.2.5 Properties of dust grains: Composition and size distribution

Composition of the grains

The elemental composition of interstellar dust grains can be determined by analyzing the spectral features in the extinction curve. As illustrated in Fig. 1.3, which shows typical extinction curves within the Milky Way for different values of R_V, a prominent and distinctive spectral feature is the pronounced bump centered around 2175 Å. This feature, originally identified by Stecher in 1965 [31], has been studied by Fitzpatrick & Massa in 1986 and they demonstrated that this characteristic feature can be accurately fitted using a Drude profile [32], defined by:

$$\Delta C_{ext}(\lambda) = \frac{C_0 \gamma^2}{(\lambda/\lambda_0 - \lambda_0/\lambda)^2 + \gamma^2} \tag{1.19}$$

where $\lambda_0 = 2175$ Å ($\lambda_0^{-1} = 4.60\ \mu\text{m}^{-1}$) represents the peak wavelength, characterized by a Full Width at Half Maximum (FWHM) of $0.992\ \mu\text{m}^{-1}$. It is noteworthy that the FWHM of this spectral characteristic exhibits significant variation along different lines of sight [32], while the central wavelength λ_0 remains constant. Shortly after the discovery of this feature, Stecher and Donn proposed that small graphitic carbon structures might explain this distinctive spectral profile [33]. However, this explanation does not account for the

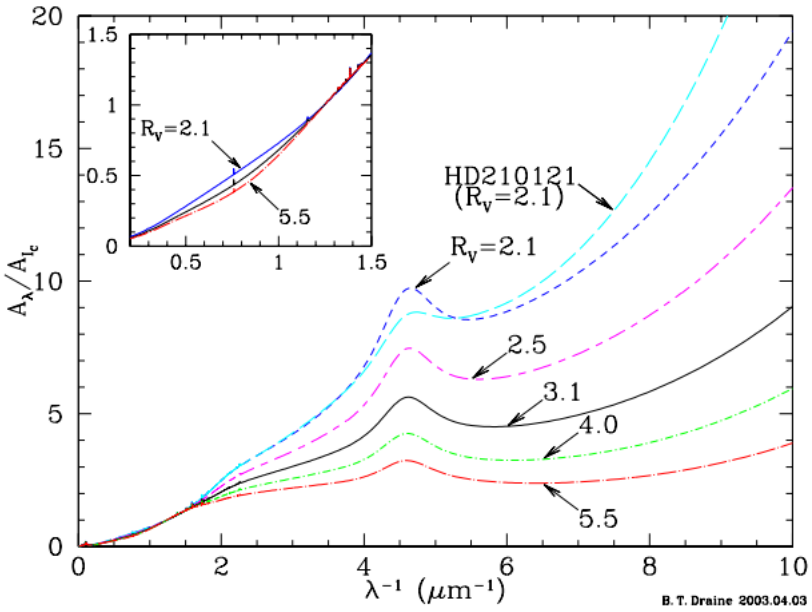

Fig. 1.3 Typical Milky Way extinction curves along different lines of sight, characterized by different values of R_V (adopted from [11])

observed variations in FWHM while maintaining a constant λ_0, as different shapes and sizes of graphitic grains lead to alterations in both FWHM and λ_0 [34]. Subsequently, numerous alternative interpretations have been proposed by researchers. Of them, the most widely accepted interpretation is derived from grain models introduced by Weingartner & Draine [35] and Li & Draine [36]. According to these models, the observed profile arises from a mixture of polycyclic aromatic hydrocarbons (PAHs), with variations in FWHM attributed to differences in the PAH composition along various lines of sight. In a recent study by [37], where they investigated a potential link between the 2175 Å UV extinction feature and PAH emission wavelengths, based on a sample of hot stars of spectral class A2 and earlier, which exhibited significant UV absorption around 2175 Å and PAH emission in the IR, observed significant shifts in the central wavelength of the 2175 Å bump, especially for stars with PAH emission, with a standard deviation of 63.9 Å, contrasting with the previously observed almost constant central wavelength. For stars without PAH emission, the shift was smaller, with a standard deviation of 24.2 Å. Shifts were also noted in the PAH emitting IR bands, and a statistically significant correlation was found between these UV and IR shifts. The shifts depend on the stellar temperature, becoming more redshifted as the stellar temperature decreases, and become more prominent below $\simeq$ 15,000 K. Stars showing redshifted UV absorption also exhibited redshifted IR emission. This pattern of UV and IR shifting with decreasing stellar temperature suggests a common origin for the 2175 Å UV absorption

feature and the IR band emissions, which are believed to be the PAH molecules.

Another prominent absorption feature in the extinction curve becomes evident in the IR region, peaking approximately at 9.7 μm. This distinctive feature is attributed to the absorption by interstellar silicates, as strong absorption features are observed near 10 μm due to the Si-O stretching mode in silicates. Further validation arises from the observation that 10 μm emission features are detected in the outflows of oxygen-rich stars, where silicates are known to form, while these features are notably absent in carbon-rich stars, where oxygen is primarily locked up in CO molecules, resulting in the absence of this particular feature. Remarkably, the 9.7 μm silicate absorption feature in the ISM displays a broad and featureless profile, in contrast to the distinct absorption signatures seen in crystalline silicates. This characteristic suggests the amorphous nature of interstellar silicates. Laboratory experiments have successfully replicated the creation of amorphous silicates through various methods, including ion bombardment of crystalline materials [38], as well as their formation in smokes [39] and other processes. The striking similarities between laboratory-derived absorption profiles and those observed in the interstellar environment strongly indicate the prevalence of amorphous silicates in interstellar grains. However, it's worth noting that the presence of a crystalline fraction cannot be entirely ruled out, especially in the circumstellar disks around young stars, crystalline silicates rich in Mg are observed [40].

Within dense molecular clouds, an additional distinctive absorption feature emerges at 3.1 μm. This particular characteristic is attributed to the O-H stretching mode occurring within solid H_2O or ice. Notably, within the Taurus dark cloud complex, an intriguing correlation has been observed: regions with $A_V > 3.3$ exhibit the presence of ice coatings or mantles on dust grains, whereas in areas with $A_V < 3.3$, dust grains lack these ice mantles [41]. In addition to this prominent ice feature, several less pronounced features arise due to the presence of H_2O and other species such as CO_2, NH_3, CO, CH_3OH, CH_4, and more. It's important to highlight that the composition of these ice mantles is highly sensitive to the local environmental conditions and their historical context.

In the wavelength range spanning from 3 to 15 μm, we observe strong emissions emanating from many emission and reflection nebulae. Strikingly, the intensity of these emissions surpasses what would be expected from thermal emissions originating in dust grains, heated by the prevailing radiation field. These emissions are primarily concentrated in five distinct peaks positioned at 3.3 μm, 6.2 μm, 7.7 μm, 8.6 μm, and 11.3 μm. These distinctive peaks are attributed to the optically active vibrational modes within PAH molecules [42]. The

presence of these optically active vibrational modes is particularly notable when hydrogen atoms are bonded to an aromatic ring [43]. It's worth mentioning that these emissions at different wavelengths correspond to specific modes: the C-H stretching mode at 3.3 μm, two instances of the C-C stretching mode at 6.2 μm and 7.7 μm, the C-H in-plane bending mode at 8.6 μm, and the C-H out-of-plane bending mode in cases where no adjacent hydrogen atom is present, occurring at 11.3 μm.

Based on the preceding discussions, several candidate materials emerge as the potential constituents of interstellar dust:

- Silicates: Silicates constitute a substantial portion of interstellar dust. While within the ISM, approximately 95% of silicates exist in an amorphous state [44], there are instances, such as in some circumstellar disks and Herbig Ae/Be stars, where a fraction of silicates exhibits a crystalline form. Although some uncertainty surrounds the precise composition of interstellar silicates, olivine ($MgFeSiO_4$) approximates a suitable composition for these dust grains [45].

- Carbonaceous Materials: This category encompasses materials primarily composed of carbon, including diamond, graphite, amorphous or glassy carbon, hydrogenated amorphous carbon, PAH, and aliphatic carbons.

- Silicon Carbide (SiC): SiC grains are primarily observed in meteorites and exhibit an emission feature at 11.3 μm in the spectra of carbon stars [46]. The absence of the 11.3 μm feature in interstellar extinction spectra suggests that the Si content in SiC dust is less than 5% of the Si content in silicates [47]. Consequently, SiC does not constitute a major component of interstellar dust grains.

- Carbonates: Calcite ($CaCO_3$) and dolomite ($CaMg(CO_3)_2$) have been detected in the dusty disks associated with some planetary nebulae [48]. However, their contribution to the total dust mass is minimal, accounting for less than 1%.

Size distribution

Given that the extinction curve serves as the primary source of information regarding dust grain properties, Mathis, Rumpl & Nordsieck employed a dust model with a combination of spherical particles composed of graphites and silicates to replicate the observed extinction curve, spanning from the UV to the NIR regions [49]. They employed a non-parametric approach to optimize the size distribution, utilizing constraints on the minimum (a_{min}) and maximum (a_{max}) grain sizes. Their findings revealed a power-law distribution, with $a_{min} \approx$

0.005 μm and $a_{max} \approx 0.25$ μm, providing the best fits. This distribution, famously known as the 'MRN' size distribution, gained prominence. However, it's worth noting that the MRN distribution did not consider the presence of PAHs, which are now known to contribute significantly to the observed extinction in the UV region.

Recent dust models [35, 50, 51] have incorporated the contributions of PAH molecules alongside carbonaceous and silicate dust to fit the extinction curve by employing diverse size distributions. It has been observed that a broad range of dust grain sizes is necessary to replicate the rise in the extinction curve from IR to the UV regions. Approximately 50% of the total ISM dust mass originates from grains with sizes below ~ 0.1 μm [7]. The current scenario suggests that dust grains within the size range of 0.05 $\mu\text{m} < a < 0.3$ μm are indispensable for producing extinction effects in the visible range of the electromagnetic spectrum within the ISM. Nevertheless, several processes within the ISM are likely to influence the grain size distribution, with an equilibrium between grain coagulation and the destruction of dust grains through collisions [52, 53]. In reality, sub-micron sized dust grains have the potential to coalesce in dense ISM regions, such as circumstellar disks, molecular clouds etc. to form larger particles [40]. Consequently, estimating the complete size distribution efficiently relies not only on the UV-optical extinction curve of the ISM but also on infrared emissions, complemented by measurements of elemental depletions within the ISM [42, 54–56].

1.2.6 Deriving the properties of dust grains from diffuse emissions

Diffuse emissions emanating from celestial objects span the entire electromagnetic spectrum, encompassing radio waves to γ-rays. These diverse emissions arise from distinct processes and mechanisms associated with different wavelengths. In the radio wavelength range, precisely at 21 cm, diffuse emission stems from HI. This emission results from the hyperfine transition within the ground state, involving two spin states, either parallel or anti-parallel. Moving to the NIR and FIR regimes, diffuse emissions originate from the thermal re-emission of radiation by dust grains. These grains are heated through the absorption of shorter-wavelength starlight. Within the optical range, much of the observed diffuse emission arises from the scattering of sunlight by the interplanetary medium, commonly referred to as zodiacal light. In the X-ray, UV, and optical spectra, starlight scatters off interstellar dust grains, forming the basis of the observed diffuse background. This thesis significantly focuses on characterizing interstellar dust grain properties. As a result, the study primarily concentrates on wavelengths where interstellar dust grains contribute significantly, especially in the FUV and IR ranges. In the FUV, the influence of zodiacal light and atomic continuum

is negligible, allowing for the observation of pure dust-scattered light. The scarcity of FUV-emitting sources offers an advantage for studying exceedingly faint diffuse sources. The observations of diffuse emissions in the FUV facilitate the derivation of two crucial optical properties of dust grains: albedo (α) and asymmetry factor (g). These parameters play a pivotal role in the investigation of interstellar dust, as they are intricately linked to the composition, size, and shape of the grains. Since absorption complements scattering, the combination of FUV and IR observations enables the comprehensive understanding of dust grain properties. In essence, these observations provide a holistic view of the characteristics of dust grains.

1.3 Multi-wavelength observations

Earth's atmosphere poses a challenge in conducting multi-wavelength observations. It selectively transmits specific wavelengths, such as optical and radio, while absorbing and scattering others like UV and IR. Ground-based observations are suitable for wavelengths that pass through the atmosphere, providing information about celestial objects. Nonetheless, for wavelengths impeded by atmospheric interference, space-based observatories become indispensable. Notably, in the optical range too, space-based observations are preferred due to the effects of atmospheric turbulence on ground-based observations. Since this thesis centers mostly around UV and IR observations, a concise introduction to several key space-based observatories, whose data have been utilized in our work, are presented in this section. For UV, we have used the data obtained with *AstroSat*, an introduction of which is presented in Sec. 2.2.1 of Chapter 2, here we present the IR observatories we have used.

- ***Spitzer Space Telescope***: The *Spitzer Space Telescope*, launched by NASA in 2003, was conceived as the IR counterpart to the renowned *Hubble Space Telescope (HST)*, originally designed for a 2.5 year mission life. It employed liquid helium for cooling its detectors, enabling the study of the early Universe and young galaxies. *Spitzer* is equipped with three instrumental payloads: the Infrared Array Camera (IRAC), the Infrared Spectrograph (IRS), and the Multiband Imaging Photometer for Spitzer (MIPS). In our work, we have utilized data observed by IRAC and MIPS. IRAC, a four-channel camera, facilitated simultaneous observations at four distinct wavelengths: 3.6 μm, 4.5 μm, 5.8 μm, and 8 μm. Each of its detectors is of 256 $\times$ 256 pixels in size, with a pixel size measuring 1.2$''$ $\times$ 1.2$''$ [57]. Meanwhile, MIPS conducted imaging and photometric observations across three broad spectral bands, employing three unique array detectors: 128 $\times$ 128 pixels at 24 μm with pixels measuring 2.45$''$ $\times$ 2.45$''$, 32 $\times$ 32 pixels at 70 μm with a pixel size of 4.0$''$ $\times$ 4.0$''$, and 2 $\times$ 20 pixels at

160 μm, each pixel covering $8.0'' \times 8.0''$ [58]. The IRS instrument delivered low and high-resolution spectra of celestial objects within the mid-infrared wavelength range (5 - 40 μm) [59].

- ***Herschel Spcae Observatory***: The *Herschel Space Observatory*, launched by the European Space Agency (ESA) in 2009, is another significant IR telescope. Its primary mission was to investigate the properties of cool celestial objects within the universe and the solar system. This included the study of star and galaxy formation and evolution, as well as their interactions with the ISM. *Herschel* stands out due to its remarkably large main mirror, spanning 3.5 meters, making it the largest among all the infrared space telescopes. Notably, it expanded observations from FIR to sub-millimeter wavelengths, providing insights deeper into the FIR spectrum. *Herschel* was equipped with three key scientific payloads: the Photoconductor Array Camera and Spectrometer (PACS), the Spectral and Photometric Imaging Receiver (SPIRE), and the Heterodyne Instrument for the Far Infrared (HIFI). PACS employed two Ge:Ga photoconductor arrays, each with dimensions of 16 $\times$ 25 pixels, as well as two filled silicon bolometer arrays with sizes of 16 $\times$ 32 pixels and 32 $\times$ 64 pixels. This configuration enabled both spectroscopy and photometry within the wavelength range of 60 - 210 μm. In photometry mode, it could simultaneously capture images in two bands: 60 - 85 μm or 85 - 125 μm, and 125 - 210 μm, all within a field of view measuring approximately $1.75' \times 3.5'$. When operating in spectroscopy mode, PACS could image a field of $47'' \times 47''$, divided into a grid of 5 $\times$ 5 pixels. This mode offered a spectral coverage of around 1500 km/s and a spectral resolution of approximately 175 km/s [60]. SPIRE, on the other hand, functioned as *Herschel*'s sub-millimeter camera and spectrometer. It comprised of an imaging photometer capable of simultaneous observation in three bands: 250 μm, 350 μm, and 500 μm, all within a field of view measuring $4' \times 8'$. Additionally, it included an imaging Fourier Transform spectrometer that could simultaneously operate across a wavelength range from 194 to 671 μm, with an approximate circular field of view spanning $2.6'$ in diameter [61]. The HIFI instrument was designed to work in two distinct wavelength bands: 157 - 212 μm and 240 - 625 μm. It consisted of a set of 7 electronically tunable heterodyne receivers, enabling the electronic separation of radiation at different wavelengths [62]. In this thesis, we have utilized archival data obtained from the PACS instrument.

1.3.1 Interstellar Medium in dwarf galaxies

The ISM found within dwarf galaxies differs notably from that present in other galaxy classifications, like spirals. A distinguishing feature of the ISM in dwarf galaxies is their low metallicity environment, setting them apart significantly from the ISM prevalent in high metallicity spiral galaxies. In these dwarf galaxies, the ISM is primarily dominated by HI [63]. Several radio wavelength surveys ($\lambda = 21$ cm) have been conducted to explore the HI properties in these dwarfs, including FIGGS (Faint Irregular Galaxies GMRT Survey) [64], THINGS (The HI Nearby Galaxy Survey) [65], SHIELD (Survey of HI in Extremely Low Mass Dwarfs) [66], among others. The surveys have detected HI in the majority of the observed dwarf galaxies. In dwarf irregular galaxies, the spatial arrangement of HI is patchy [67, 68], unlike the organized distribution of the ISM in the arms of spiral galaxies. The emission peaks of individual HI clouds are typically situated in proximity to active star-forming regions within a galaxy [69, 70]. For star formation to occur, a minimum HI column density, N(HI) $\sim 10^{21}$ cm^{-2}, is generally required [71, 72]. However, certain galaxies exhibit HI density peaks surpassing this threshold without concurrent recent star formation activity [67]. This suggests the necessity of a triggering mechanism to initiate the star formation process in these cases.

In the ISM, the presence of dust grains depends on the availability of metals [73]. In environments characterized by low metallicity (12+log(O/H) < 8.0), the formation of dust grains faces challenges due to the harsh, unshielded conditions within the ISM. Consequently, the dust-to-gas mass ratio diminishes more rapidly than the oxygen abundance in such settings [74]. Conversely, in metal-rich environments, the abundance of dust grains tends to grow approximately proportionally to the oxygen abundance [75, 76]. A distinct characteristic of the low-metallicity ISM in dwarf galaxies is the limited emission from PAH molecules [77]. This stands in contrast to the substantial PAH emissions observed in the ISM of high-metallicity galaxies.The prominent emission peaks of PAHs are observed at 6.2 μm, 7.7 μm, 8.6 μm, 11.3 μm, and 12.7 μm. The deployment of the *Spitzer Space Telescope* not only confirmed the scarcity of PAH emission in low metallicity environments but also revealed a trend of diminishing PAH emission with decreasing metallicity [75, 78, 79], establishing a threshold in metallicity below which PAH abundance sharply declines. A comprehensive study by [80] analyzing *Spitzer* 8 μm and 24 μm emissions from 34 galaxies over two decades, demonstrated a shift in the ratio of 8 μm to 24 μm emission from ~ 0.7 for galaxies with $Z/Z_\odot > 1/3$ to ~ 0.08 for galaxies with $Z/Z_\odot < 1/5$ - 1/3. This shift was attributed to a significant decrease in 7.7 μm PAH emission, occurring at a threshold metallicity of 12 + log(O/H) $\approx$ 8.2. The precise cause for the scarcity of PAH in low metallicity environments

remains unclear. A commonly proposed explanation is the photodissociation of PAH by intense UV radiation in these environments, where there is an inadequate presence of dust grains to shield the PAH molecules from UV radiation [81]. Another possibility is the more effective destruction of PAH through thermal sputtering in shock-heated gas that cools more slowly due to reduced metallicity. The lack of PAH might also be attributed to a deficiency of PAH-producing carbon stars and carbon-rich planetary nebulae, or a hindered formation and growth of PAH in an ISM with low gas-phase carbon abundance [82].

1.3.2 Star formation in dwarf galaxies

In large galaxies like the Milky Way, continuous star formation occurs at numerous active sites. While the specific locations of these star-forming regions may change over time, their overall number and star formation rate (SFR) have remained relatively constant over a span of a few billion years [83, 84]. However, the situation is different for dwarf galaxies. In the dwarfs of the Local Group, the star formation history exhibits spikes [85]. Each galaxy has a unique individual star formation history. Galaxies with recent star formation activity show intermittent periods of enhanced activity, reflecting the bursty nature of star formation in dwarf galaxies [86–88].

The SFR within a galaxy can be inferred from the FUV emission. The SFR derived from FUV luminosity corresponds to an equilibrium timescale of approximately 10^8 years for bursty star formation [89]. Analysis of *HST* data on AGB and helium-burning stars has unveiled highly individual star formation histories over the last 10^8 years in 23 dwarf galaxies from the Legacy Extragalactic UV Survey (LEGUS) [90]. In about half of these galaxies, a spatial progression of star formation is also observed, a phenomenon similarly noted in the dwarf galaxies of the M81 group [91]. Major bursts, exceeding a factor of three over the average during the specified time interval, are not observed. This finding aligns with the study by [89] which compared Hα (timescale: $\approx$ 5 Myr) and UV emission (timescale: 10^8 years) for 185 local galaxies. Dwarfs near the upper luminosity limit ($M_V \approx -18$) show burst amplitudes not exceeding a factor of ten with respect to the average SFR, while galaxies below $M = 10^{7.5} M_\odot$ may undergo substantial and rapid bursts, reaching amplitudes up to two orders of magnitude over the average SFR within a timescale of less than 30 Myr.

During short periods of ongoing starbursts, Hβ and UV luminosities are expected to exhibit considerable enhancement. Hβ emission is anticipated to decrease more rapidly than UV emission since Hβ is emitted by younger and more massive stars. In a study by [92], approximately 14,000 compact star-forming galaxies at redshifts $z \sim 0$ - 1 from the

Sloan Digital Sky Survey (SDSS) were investigated. The study revealed rapid fluctuations in Hβ and UV luminosities on a timescale of a few million years, indicating that star formation occurs in short, intense bursts. The contribution from continuous star formation to these luminosities was found to be very low, if present. Extrapolating these Hβ and UV luminosities to the time when the burst was at its peak (zero age), the study found that the SFR in these galaxies was tightly and linearly correlated with stellar mass. Additionally, the specific SFR (the ratio of SFR to stellar mass) was observed to be independent of galactic stellar mass. In summary, the key distinction between star formation in large galaxies and dwarf galaxies lies in the nature of the process. In large galaxies, star formation occurs at a continuous rate, while in dwarfs, it is characterized by bursty episodes.

1.4 Cosmological importance of dwarf galaxies

The resemblance of a metal-poor ISM with a low dust content in dwarf galaxies [1] to the features observed in early Universe galaxies is noteworthy. Recent observations of luminous galaxies at redshifts $z > 10$, initially conducted by *HST* and later by the *James Webb Space Telescope* (JWST), have brought attention to the scarcity of dust in a subset of these high-redshift galaxies [93, 94]. In light of these findings, dwarf galaxies emerge as crucial analogs that may replicate early Universe conditions. Analyzing both Local Group and nearby group dwarf galaxies on smaller scales becomes essential to gain valuable insights into the diverse physical processes of more distant dwarf galaxies and early galaxies. A comparative analysis of the overall emission characteristics and properties of these dwarf galaxies can provide significant understanding of the evolutionary trajectory from early Universe galaxies to their contemporary counterparts.

1.5 Objectives and outline of the thesis

In this thesis, as the title suggests, we study different aspects of the ISM of two metal poor dwarf irregular galaxies from Local Group as well as nearby groups: Holmberg II from the galaxy group M81 and the Large Magellanic Cloud from the Local Group.

In **Chapter 2**, we describe our UV observations and data reduction of Holmberg II obtained with the Ultra Violet Imaging Telescope (UVIT) instrument onboard first Indian multi-wavelength space mission *AstroSat*. We also highlight the significant improvement in the resolution of *AstroSat*/UVIT compared to its predecessors.

Holmberg II hosts one of the brightest ultra luminous X-ray (ULX) sources in the local Universe. These ULX sources exhibit high variability in X-ray emissions and also emit prominently in the UV spectrum. Notably, the UV emissions result from the reprocessing of X-ray photons. So, one should expect an UV/X-ray correlation. In **Chapter 3**, we present the X-ray observations of the ULX source, taken simultaneously with the UV observations. We try to find the correlation between X-ray and UV flux variations from the source. Further, we try to describe the correlation in terms of three models and also estimated the lower limit of the variability required to reject at least a part of them.

We move towards investigating the ISM within Holmberg II in **Chapter 4**, utilizing high resolution UV observations from the *AstroSat*/UVIT instruments, complemented by IR data from the *Spitzer* and *Herschel* space telescopes. This chapter focuses on examining the interstellar dust component specifically within the galaxy. Interstellar dust plays a pivotal role, scattering a portion of shorter wavelength radiations and manifesting as diffuse emissions primarily in the FUV range. They also absorb the remaining portion of these shorter wavelengths (mainly UV and optical) and subsequently re-emit in longer wavelengths, mainly in the MIR and FIR ranges. Our investigation unfolds in three key parts: the initial part centers on analyzing the correlation between UV and IR emissions within Holmberg II, determining the nature of dust grains contributing to the diffuse emissions. The subsequent part delves into studying the diffuse FUV emission attributable to dust scattering in the galaxy. This investigation involves modeling using an established single scattering model [95], allowing us to derive crucial dust optical properties — specifically, the albedo (α) and asymmetry factor (g). Lastly, we probe the diffuse IR emission attributed to thermal re-emission by dust grains heated through UV/optical photons. This aims to uncover distinct dust populations characterized by varying temperatures within Holmberg II.

In **Chapter 5**, we turn our attention to the second sample of our study — the Large Magellanic Cloud — with a specific focus on examining the interstellar dust component within it. Within the galaxy, we directed our study towards one of its prominent H II regions: 30 Doradus, also known as the Tarantula Nebula. Previously, [96] undertook observations of FUV diffuse emissions across various regions of the galaxy using the *Far Ultraviolet Spectroscopic Explorer* (*FUSE*) telescope, in seven distinct wavelength bands ranging from 1004 Å to 1159 Å. Additionally, a previous UV-IR correlation study for 30 Doradus was conducted by [97]. Building upon these foundations, our approach shifted towards modeling the diffuse FUV emission within 30 Doradus, utilizing the same scattering model employed in Chapter 4.

Finally in **Chapter 6**, we summarize the thesis with its implications and looking towards the future, particularly in the context of alternative sources of diffuse UV emission apart from dust scattering.